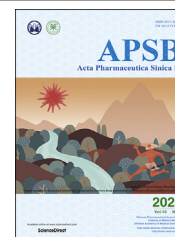




Chinese Pharmaceutical Association
Institute of Materia Medica, Chinese Academy of Medical Sciences

Acta Pharmaceutica Sinica B

www.elsevier.com/locate/apsb
www.sciencedirect.com



ORIGINAL ARTICLE

Discovery of a highly selective VEGFR2 kinase inhibitor CHMFL-VEGFR2-002 as a novel anti-angiogenesis agent



Zongru Jiang^{a,b,†}, Li Wang^{a,b,†}, Xuesong Liu^{a,b,†}, Cheng Chen^{a,b,†},
Beilei Wang^{a,b}, Wenliang Wang^{a,b}, Chen Hu^a, Kailin Yu^a, Ziping Qi^a,
Qingwang Liu^c, Aoli Wang^a, Jing Liu^{a,d}, Guangchen Hong^{e,*},
Wenchao Wang^{a,d,*}, Qingsong Liu^{a,b,c,d,f,*}

^aHigh Magnetic Field Laboratory, Key Laboratory of High Magnetic Field and Ion Beam Physical Biology, Hefei Institutes of Physical Science, Chinese Academy of Sciences, Hefei 230031, China

^bUniversity of Science and Technology of China, Hefei 230026, China

^cPrecision Targeted Therapy Discovery Center, Institute of Technology Innovation, Hefei Institutes of Physical Science, Chinese Academy of Sciences, Hefei 230088, China

^dPrecision Medicine Research Laboratory of Anhui Province, Hefei 230088, China

^eQingdao Shinan District People's Hospital, Qingdao 266002, China

^fInstitutes of Physical Science and Information Technology, Anhui University, Hefei 230601, China

Received 7 May 2019; received in revised form 12 September 2019; accepted 27 September 2019

KEY WORDS

Cancer;
VEGFR2 kinase;
Kinase inhibitor;
Angiogenesis;
Inhibitor selectivity

Abstract Angiogenesis is an essential process in tumor growth, invasion and metastasis. VEGF receptor 2 (VEGFR2) inhibitors targeting tumor angiogenic pathway have been widely used in the clinical cancer treatment. However, most of currently used VEGFR2 kinase inhibitors are multi-target inhibitors which might result in target-associated side effects and therefore limited clinical toleration. Highly selective VEGFR inhibitors are still highly demanded from both basic research and clinical application point of view. Here we report the discovery and characterization of a novel VEGFR2 inhibitor (CHMFL-VEGFR2-002), which exhibited high selectivity among structurally closed kinases including PDGFRs, FGFRs, CSF1R, etc. CHMFL-VEGFR2-002 displayed potent inhibitory activity against VEGFR2 kinase in the biochemical assay ($IC_{50} = 66$ nmol/L) and VEGFR2 autophosphorylation in cells (EC_{50} s ~ 100 nmol/L) as well as potent anti-proliferation effect against VEGFR2 transformed BaF3 cells

*Corresponding authors. Tel.: +86 551 65595161; fax: +86 551 65591485.

E-mail addresses: qsliu97@hmfl.ac.cn (Qingsong Liu), wwcbox@hmfl.ac.cn (Wenchao Wang), 2297023869@qq.com (Guangchen Hong).

[†]These authors made equal contributions to this work.

Peer review under the responsibility of Chinese Pharmaceutical Association and Institute of Materia Medica, Chinese Academy of Medical Sciences.

<https://doi.org/10.1016/j.apsb.2019.10.004>

2211-3835 © 2020 Chinese Pharmaceutical Association and Institute of Materia Medica, Chinese Academy of Medical Sciences. Production and hosting by Elsevier B.V. This is an open access article under the CC BY-NC-ND license (<http://creativecommons.org/licenses/by-nc-nd/4.0/>).

(GI₅₀ = 150 nmol/L). In addition, CHMFL-VEGFR2-002 also displayed good anti-angiogenesis efficacy *in vitro* and exhibited good *in vivo* PK (pharmacokinetics) profile with bioavailability over 49% and anti-angiogenesis efficacy in both zebrafish and mouse models without apparent toxicity. These results suggest that CHMFL-VEGFR2-002 might be a useful research tool for dissecting new functions of VEGFR2 kinase as well as a potential anti-angiogenic agent for the cancer therapy.

© 2020 Chinese Pharmaceutical Association and Institute of Materia Medica, Chinese Academy of Medical Sciences. Production and hosting by Elsevier B.V. This is an open access article under the CC BY-NC-ND license (<http://creativecommons.org/licenses/by-nc-nd/4.0/>).

1. Introduction

Angiogenesis, the formation of new blood vessels from preexisting vasculature is one of the hallmarks of cancerous growth^{1,2}. When new blood vessels grow in tumors, they provide tumors with essential nutrients and oxygen to sustain tumor growth³. Tumor angiogenesis is also an essential process for tumor invasion and metastasis⁴. So anti-angiogenesis is one of the main strategies for treatment of cancers⁵. Among the many of the angiogenic factors, vascular endothelial growth factor (VEGF) has been identified as the most critical factor in regulating normal physiological and tumor angiogenesis^{6,7}. The pro-angiogenic signaling molecule VEGF comprises seven secreted glycoproteins due to splicing variation, and VEGFR receptors include VEGFR-1 (Flt1), VEGFR-2 (KDR), VEGFR-3 (Flt4) and the neuropilins (NP-1 and -2) with different functions in various cell types⁸. VEGF and its receptors induce proliferation migration and tube formation in endothelial cells⁹. Among them, receptor VEGFR2 is mainly responsible for cell proliferation, vascular permeability, cell migration, and cell survival through VEGF-induced signaling in endothelial cells¹⁰.

Therefore, VEGFR2 is considered as an important therapeutic target for anti-angiogenesis therapy in most solid tumors. U.S. Food and Drug Administration (FDA) has already approved anti-VEGFR2 agents for the treatment of multiple tumors^{7,11}. Several orally active small-molecule tyrosine kinase inhibitors of VEGFR2 are now in clinical use such as sunitinib¹², sorafenib¹³, apatinib¹⁴, lenvatinib¹⁵, tivozanib¹⁶, etc. In addition, many candidate drugs were tested in clinical trials, such as lucitanib¹⁷, vatalanib¹⁸, etc. VEGFR2 inhibitors have become an important arsenal in the treatment of various types of cancers, including renal cell carcinoma (RCC), gastrointestinal stromal tumor

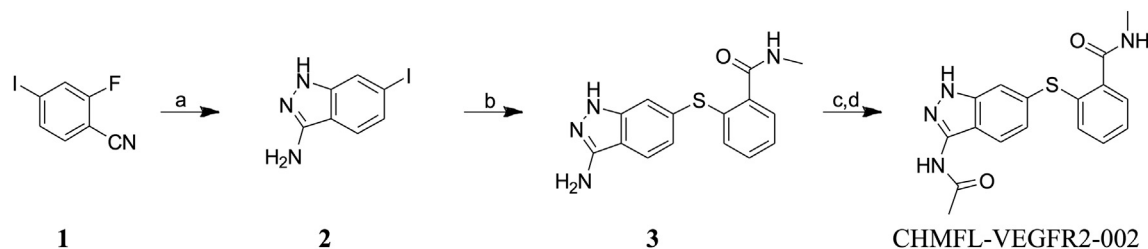
(GIST), hepatocellular carcinoma (HCC) and leukemia. However, serious side effects associated with currently available anti-VEGF agents limited their long-term usage^{19,20}, and there is growing evidence that sunitinib causes abnormalities in thyroid function^{21–23}. In addition, some multi-target VEGFR2 inhibitors have been found to have myelosuppression side effects²⁴. Therefore, new VEGFR2 inhibitors with safer treatment window are still in great demand.

In this study, to achieve less toxicity of VEGFR2 inhibitors, we discovered a new highly selective VEGFR2 inhibitor CHMFL-VEGFR2-002 by high-throughput screening of our in-house generated small molecule library. CHMFL-VEGFR2-002 displayed potent and specific inhibition of VEGFR2 tyrosine kinase activity *in vitro*, and efficiently inhibited angiogenesis *in vitro* and *in vivo*, suggesting that this compound might become a potential angiogenesis inhibitor and a tool for studying VEGFR2.

2. Result and discussion

2.1. CHMFL-VEGFR2-002 inhibits VEGFR2 kinase activity *in vitro*

To discover a highly selective VEGFR2 inhibitor, we screened a house-made kinase inhibitor library using VEGFR2-transformed BaF3 cells (Supporting Information Table S1) and we found CHMFL-VEGFR2-002 as a potent VEGFR2 inhibitor. The synthetic route of CHMFL-VEGFR2-002 was shown in Scheme 1. To characterize the activity of CHMFL-VEGFR2-002 against VEGFR2 kinase, we expressed VEGFR2 protein and performed kinase inhibition assays. As shown in Fig. 1A, CHMFL-VEGFR2-002 inhibited VEGFR2 kinases with high potency (IC₅₀ = 66 nmol/L). In BaF3 cell lines, CHMFL-VEGFR2-002



Scheme 1 Synthetic route of compound CHMFL-VEGFR2-002. Reagents and conditions: (a) hydrazine hydrate, *t*-BuOH, 115 °C, 5 h; (b) 2-mercapto-*N*-methylbenzamide, Pd₂(dba)₃, xantphos, Na₂CO₃, DMF, 80 °C, 14 h; (c) acetyl chloride, DMF, DIPEA, 0 °C–r.t., 8 h; (d) 1,2-DAP, THF, 60 °C, 6 h.

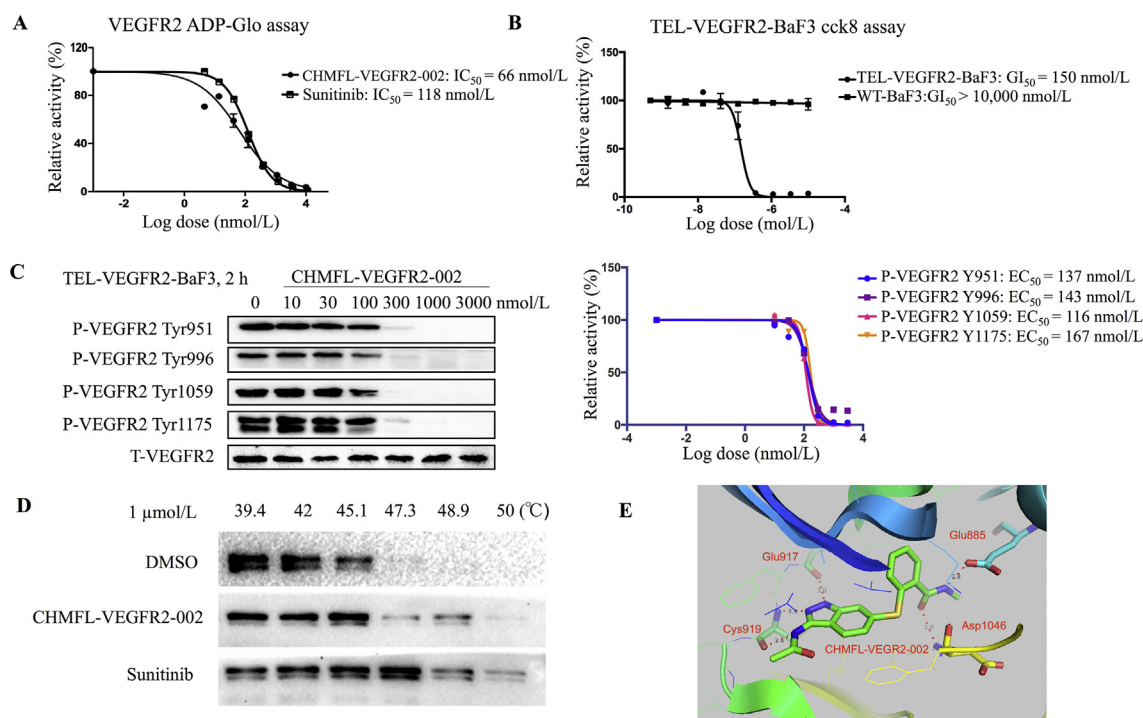


Figure 1 CHMFL-VEGFR2-002 inhibits VEGFR2 activity. (A) IC_{50} determination of CHMFL-VEGFR2-002 with purified VEGFR2 kinase protein using the ADP-Glo assay. (B) GI_{50} determination of CHMFL-VEGFR2-002 with TEL-VEGFR2-BaF3 cells using the CCK8 assay. (C) EC_{50} determination of CHMFL-VEGFR2-002 on auto-phosphorylation of VEGFR2 in TEL-VEGFR2-BaF3 cells. (D) The cellular on-target effect of CHMFL-VEGFR2-002 using the Cellular Thermal Shift Assay. (E) Docking of CHMFL-VEGFR2-002 into VEGFR2 kinase X-ray crystal structure (PDB ID: 4AG8).

was highly potent for inhibition of the proliferation of Tel-VEGFR2-BaF3 cells ($GI_{50} = 150$ nmol/L, Fig. 1B). In order to further confirm the on-target effect of CHMFL-VEGFR2-002, we then examined its effect for the blockage of VEGFR2 auto-phosphorylation in VEGFR2 transformed BaF3 isogenic cell lines. The results demonstrated that upon 2 h of CHMFL-VEGFR2-002 treatment, the phosphorylation of VEGFR2 at Y951, Y996, Y1059 and Y1175 residues was significantly inhibited in TEL-VEGFR2-BaF3 cells ($EC_{50} = 137, 143, 116$ and 167 nmol/L, respectively, Fig. 1C). Therefore, CHMFL-VEGFR2-002 can effectively inhibit the VEGFR2 signaling pathway. In addition, we further detected the inhibition of CHMFL-VEGFR2-002 on VEGFR2 through the Cellular Thermal Shift Assay, the results showed that it could significantly stabilize the protein with increasing temperature (from 39.4 to 50 $^{\circ}\text{C}$, Fig. 1D). In order to further understand the detailed binding mechanism, we then docked CHMFL-VEGFR2-002 into the X-ray structure of VEGFR2 kinase (PDB ID: 4AG8)²². The results showed that the compound adopted a typical type II binding mode with VEGFR2 kinase, which is similar to sunitinib²⁵. The indazole amine moiety of compound formed three hydrogen bonds with Cys919 and Glu917 in the hinge binding area. Two canonical hydrogen bonds were formed between the methyl benzamide moiety and the Glu885 and Asp1046 (Fig. 1E).

In addition, to further understand the better activity of CHMFL-VEGFR2-002 over other compounds screened as listed in Table S1, we then chose three representative compounds including compounds **2**, **10** and **14** to dock them into VEGFR2

kinase (Supporting Information Fig. S4). The results showed that all of these compounds could adopt a type II binding mode which is similar to CHMFL-VEGFR2-002. The data also demonstrated that there were three key elements which contributed to the binding capability including the hydrogen bonds in the hinge binding area (Cys919 and Glu917), gatekeeper region hydrophobic pocket, and the DFG-out region hydrophobic pocket. Comparing to CHMFL-VEGFR2-002, all of compounds **2**, **10** and **14** lost one of the hydrogen bonds in the hinge binding region (Fig. S4A, C and E). In addition, compounds **10** and **14** lost the hydrophobic pocket interaction comparing to compound **2** and CHMFL-VEGFR2-002 (Fig. S4B, D, F and G). In the DFG-out region hydrophobic pocket, compounds **10** and **14** provided more hydrophobic interaction than compounds **2** and CHMFL-VEGFR2-002 (Fig. S4H). Combining all of these factors together, the more key hydrogen bonds in the hinge binding area and hydrophobic interaction in the gatekeeper region of kinase possibly gave CHMFL-VEGFR2-002 better potency than other screened compounds.

2.2. CHMFL-VEGFR2-002 is a highly selective inhibitor for VEGFR2

VEGFR kinase family comprises of three members, including VEGFR1, VEGFR2, and VEGFR3. To see whether our compound achieved selectivity among the three kinases, we examined its anti-proliferation effects on VEGFR-transformed BaF3 cells. The data showed that CHMFL-VEGFR2-002 selectively inhibited

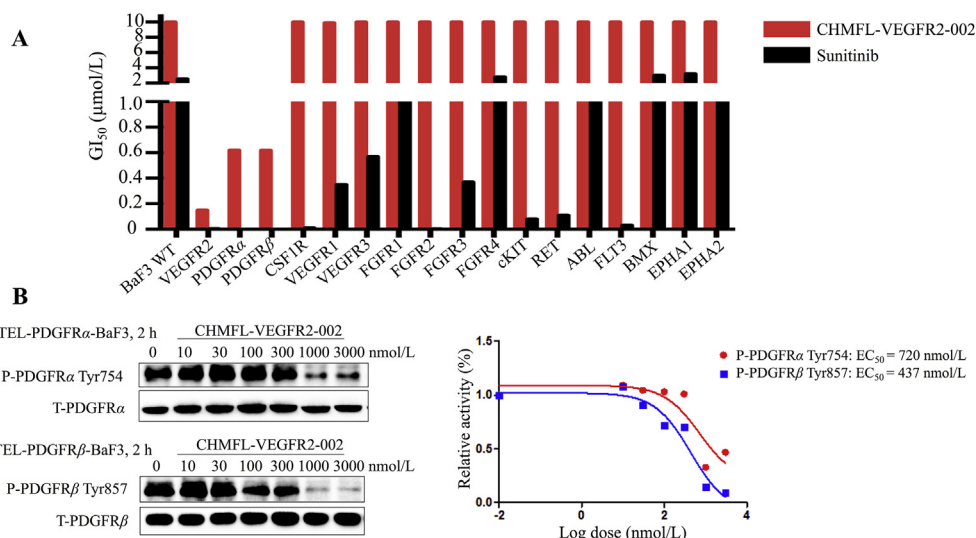


Figure 2 Characterization of CHMFL-VEGFR-002 as a high-selective VEGFR2 inhibitor. (A) The anti-proliferative effects of CHMFL-VEGFR2-002 against a panel of kinase transformed BaF3 cells with sunitinib as control. (B) The effects of CHMFL-VEGFR2-002 on auto-phosphorylation of PDGFRs in TEL-PDGFR α/β -BaF3 cells.

TEL-VEGFR2-BaF3 ($GI_{50} = 150$ nmol/L), but not TEL-VEGFR1/3-BaF3 ($GI_{50}s > 10,000$ nmol/L). In addition, since VEGFR2 shares high sequence similarity with other receptor kinases, including RET, FGFR, CSF1R and PDGFR α/β , and most of the current VEGFR inhibitors often target these kinases, we tested the compound in a panel of kinase transformed BaF3 cells. The results revealed that it was highly selective among 18 kinases (Fig. 2A and Table 1) compared with sunitinib. Besides VEGFR2, it also displayed efficacy against PDGFR α ($GI_{50} = 620$ nmol/L) and PDGFR β ($GI_{50} = 618$ nmol/L). To confirm its effects on PDGFR kinases, we also examined the phosphorylation of PDGFR α on TEL-PDGFR α -BaF3 cells ($EC_{50} = 720$ nmol/L) and phosphorylation of PDGFR β on TEL-PDGFR β -BaF3 cells ($EC_{50} = 437$ nmol/L), which showed that CHMFL-VEGFR2-002 potently inhibited VEGFR2 with 4–7-fold selectivity over PDGFR α and PDGFR β (Fig. 2B). Collectively, these results illustrated that CHMFL-VEGFR2-002 is a highly selective VEGFR2 inhibitor.

2.3. CHMFL-VEGFR2-002 inhibited VEGF-induced angiogenesis *in vitro*

HUVEC is commonly used as a cell model for angiogenesis study. To see if our compound could inhibit VEGFR2 kinase activity, we treated HUVEC cells with CHMFL-VEGFR2-002, and the results showed that VEGFR2 was phosphorylated in the DMSO group and 0.3 μ mol/L of CHMFL-VEGFR2-002 diminished VEGFR2 phosphorylation (Fig. 3A). The results from *in vitro* capillary tube formation showed that, compared with the intense capillary tube networks formed by HUVEC plated onto BD Matrigel in the control group, treatment of the cells with CHMFL-VEGFR2-002 at 3 μ mol/L induced significant reduction in the total branch lengths of tubular network structures and the formation of new tubes decreased in a concentration-dependent manner (Fig. 3B).

To see whether CHMFL-VEGFR2-002 affects VEGF-induced migration of HUVEC cells, we performed transwell invasion assays and the results showed that CHMFL-VEGFR2-002

Table 1 Anti-proliferation activity of CHMFL-VEGFR2-002 in BaF3 cell lines.

Cell line	GI_{50} (nmol/L)		Cell line	GI_{50} (nmol/L)	
	CHMFL-VEGFR2-002	Sunitinib		CHMFL-VEGFR2-002	Sunitinib
BaF3	>10,000	2560	TEL-FLT3-BaF3	>10,000	32
TEL-VEGFR2-BaF3	150	5	TEL-BMX-BaF3	>10,000	3020
TEL-PDGFR α -BaF3	620	1	BCR-DDR2-BaF3	>10,000	NA
TEL-PDGFR β -BaF3	618	<1	TEL-EPHA1-BaF3	>10,000	3210
TEL-VEGFR1-BaF3	9900	350	TEL-EPHA2-BaF3	>10,000	1270
TEL-VEGFR3-BaF3	>10,000	570	TEL-CSF1R-BaF3	>10,000	11
TEL-cKIT-BaF3	>10,000	81	TEL-FGFR1-BaF3	>10,000	1680
TEL-RET-BaF3	>10,000	110	TEL-FGFR2-BaF3	>10,000	4
TEL-ABL-BaF3	>10,000	1550	TEL-FGFR3-BaF3	>10,000	370
P210-BaF3	>10,000	1460	TEL-FGFR4-BaF3	>10,000	2820

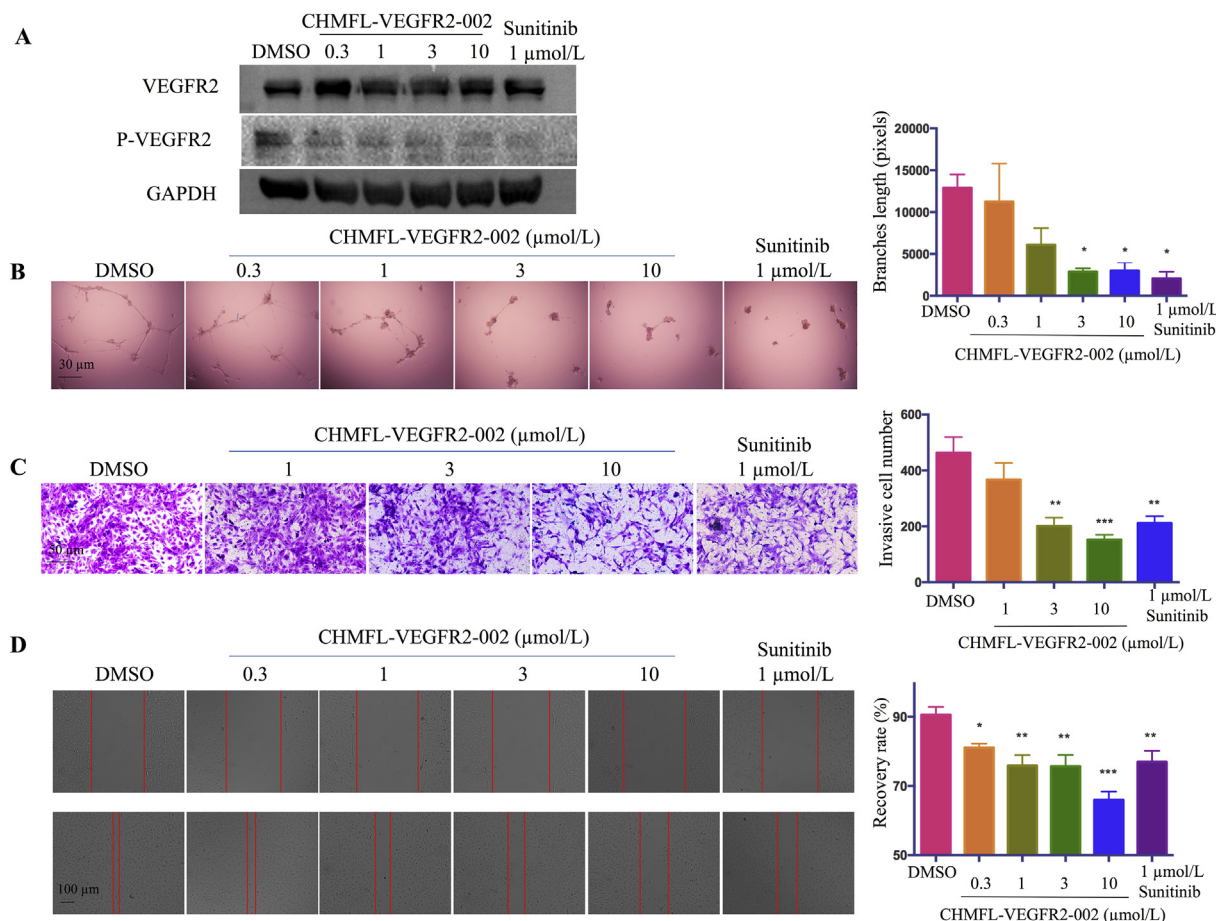


Figure 3 Anti-angiogenesis effect of CHMFL-VEGFR2-002 *in vitro*. (A) CHMFL-VEGFR2-002 inhibited phosphorylation of VEGFR2 in HUVEC cells. (B) CHMFL-VEGFR2-002 impaired capillary tube formation of HUVEC cells. HUVECs were plated on Matrigel with DMSO or various concentrations of compounds. After 24 h, tubes were photographed and measured. (C) CHMFL-VEGFR2-002 inhibited HUVEC invasion in transwell assay. 5×10^4 HUVECs were seeded in the top chamber with various concentrations of compounds. After 24 h, the invaded HUVEC cells were photographed and counted. (D) CHMFL-VEGFR2-002 inhibited HUVEC cell migration in wound healing assay. CHMFL-VEGFR2-002 group is compared with DMSO group, and significance of difference is indicated. The distance of migration is measured by ImageJ. Data are mean \pm SD ($n = 3$). * $P < 0.05$, ** $P < 0.01$, *** $P < 0.001$ versus control treatment.

suppressed the direct migration of HUVEC cells (Fig. 3C). In addition, data from wound-healing assay showed apparent migration in untreated HUVEC cells after 12 h, but the treatment of CHMFL-VEGFR2-002 and sunitinib caused less migrated HUVEC cells across the plates. The inhibition of migration in HUVEC cells by CHMFL-VEGFR2-002 was dose-dependent (Fig. 3D). These data showed that CHMFL-VEGFR2-002 can inhibit endothelial cell migration, invasion and tube formation *in vitro*, which are important steps in angiogenesis.

2.4. Pharmacokinetics of CHMFL-VEGFR2-002

To evaluate the efficacy of CHMFL-VEGFR2-002 in animal models, we first examined the pharmacokinetic profile of CHMFL-VEGFR2-002. With 10 mg/kg oral administration, the plasma concentrations (C_{max}) peaked within 30 min (T_{max}) suggesting a rapid entrance of the drug into the systemic circulation. The plasma concentrations then declined with an effective half time $t_{1/2}$ of 2.9 h for CHMFL-VEGFR2-002. The

AUC_{0–inf} (area under the curve) was 2265.7 ± 692.9 ng/mL·h for the 10 mg/kg of CHMFL-VEGFR2-002 by oral administration. Comparably, this compound displayed better PK (pharmacokinetics) profiles than sunitinib in the same formulation (Table 2). The calculated bioavailability ($F\%$) of CHMFL-VEGFR2-002 is 49%, indicating that the compound is suitable for oral administration in the *in vivo* experiments. All *in vivo* studies were approved by the Hefei Institutes of Physical Science Ethics Committee, Chinese Academy of Sciences (Hefei, China).

2.5. CHMFL-VEGFR2-002 exhibits low acute toxicity

We then evaluated the toxicity profile of this compound in animals. During acute toxicity study with ICR mice (dosed only once in the first day and continued to observe animals' behavior and body weight for 7 days), we did not observe any death and body weight loss in animals with CHMFL-VEGFR2-002 up to 2000 mg/kg dosage which indicating a low acute toxicity profile

Table 2 PKs of CHMFL-VEGFR2-002 and sunitinib.

Parameter	CHMFL-VEGFR2-002		Sunitinib	
	i.v. (1 mg/kg)	p.o. (10 mg/kg)	i.v. (1 mg/kg)	p.o. (10 mg/kg)
AUC _{0-t} (ng/mL·h)	443.292 ± 36.858	2194.607 ± 759.148	142.7 ± 40.3	927.2 ± 107.5
AUC _{0-∞} (ng/mL·h)	452.771 ± 34.465	2265.7 ± 692.912	144.8 ± 39.6	1095.9 ± 96.7
MRT _{0-t} (h)	0.956 ± 0.18	4.156 ± 1.338	0.98 ± 0.04	7.63 ± 0.30
C _{max} (ng/mL)	1331.896 ± 525.603	455.579 ± 17.611	236.0 ± 66.8	175.0 ± 21.7
T _{max} (h)	0.017 ± 0	0.5 ± 0	0.33 ± 0	1.25 ± 1.06
t _{1/2} (h)	2.416 ± 0.952	2.931 ± 0.614	1.05 ± 0.34	1.38 ± 0.46
F (%)	–	49.51	–	75.7

– Not applicable.

Table 3 Acute toxicity test of CHMFL-VEGFR2-002 and sunitinib.

Compd.	Dosage (mg/kg)	Concentration (mg/mL)	Volume (mL/mouse)	Number of deaths (death/total)
Vehicle (HKI)	0	0	0.2	♀: 0/2
CHMFL-VEGFR2-002	2000	200	0.2	♀: 0/2
	1000	100	0.2	♀: 0/2
	500	50	0.2	♀: 0/2
	250	25	0.2	♀: 0/2
	125	12.5	0.2	♀: 0/2
Sunitinib	2000	200	0.2	♀: 2/2
	1000	100	0.2	♀: 0/2
	500	50	0.2	♀: 0/2
	250	25	0.2	♀: 0/2
	125	12.5	0.2	♀: 0/2

(Table 3 and Fig. S4). Comparably, sunitinib started to show toxicity at 500 mg/kg which resulted in apparent body weight loss though it recovered starting from day 4. 1000 mg/kg single dosage of sunitinib resulted in unrecovered body weight loss and 2000 mg/kg dosage led to mice death on day 3 (Table 3 and Fig. S4).

2.6. CHMFL-VEGFR2-002 inhibits embryonic angiogenesis in zebrafish models

To test the anti-angiogenic effect of CHMFL-VEGFR2-002 *in vivo*, we used the transgenic zebrafish (kdr1:EGFP) as a rapid and visual model for the evaluation of anti-angiogenic action *in vivo*. Zebrafish embryos were incubated 72 h with CHMFL-VEGFR2-002, DMSO, and sunitinib. Digital images were captured using the fluorescence microscope and the fluorescence images showed that, similar to sunitinib, CHMFL-VEGFR2-002 strongly inhibited the formation of intersegmental vessels in a dose-dependent manner with the intersegmental vessels almost completely blocked at the concentration of 1 μmol/L (Fig. 4). Therefore, the anti-angiogenesis effect of CHMFL-VEGFR2-002 can also be demonstrated in zebrafish model.

2.7. CHMFL-VEGFR2-002 inhibits tumor growth *in vivo*

In clinic, peritoneal dissemination of tumors often indicates poor prognosis for cancer patients²⁶. To evaluate the effect of CHMFL-VEGFR2-002 on tumor dissemination, we treated the mice after intraperitoneal inoculation of MKN45 cells and found that CHMFL-VEGFR2-002 could reduce tumor numbers on the mesenterium without affecting body weights of the animals (Fig. 5A). No significant weight loss was observed when compared with the control group (Fig. 5B). In addition, B16-F10 is a malignant mouse melanoma cell line that is highly prone to metastasis. To see if CHMFL-VEGFR2-002 could prolong the overall survival of animals inoculated with B16-F10, we treated the animals through oral administration daily with the compound, and as shown in

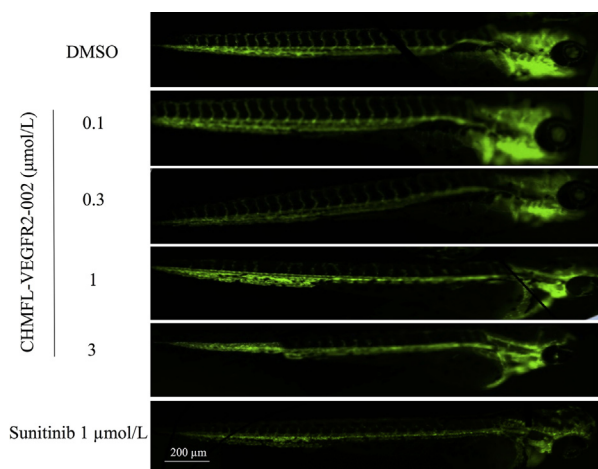


Figure 4 CHMFL-VEGFR2-002 inhibited angiogenesis in zebrafish and tumor growth. CHMFL-VEGFR2-002 inhibited the Intersegmental vessel (ISV) growth. The transgenic zebrafish (EGFP) was treated with DMSO, CHMFL-VEGFR2-002, and sunitinib.

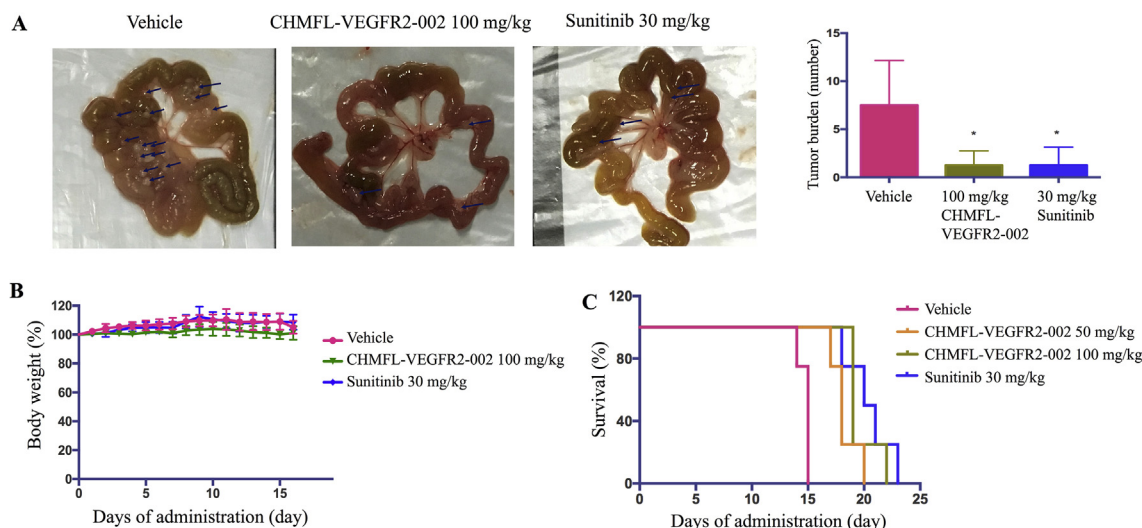


Figure 5 CHMFL-VEGFR2-002 inhibited tumor growth. (A) Anti-tumor efficacy of CHMFL-VEGFR2-002 in the peritoneal dissemination model. MKN45 cells were inoculated into nude mice and treated with DMSO, CHMFL-VEGFR2-002, and sunitinib. After 17 days, tumors in CHMFL-VEGFR2-002 group were significantly less than DMSO group (tumors are marked with arrows), $*P < 0.05$ versus control treatment. (B) Body weight monitoring of CHMFL-VEGFR2-002 in mouse xenograft model. (C) CHMFL-VEGFR2-002 increased the survival rate of C57 mice bearing B16-F10 compared with DMSO. Data are mean \pm SD ($n=5$).

Fig. 5C, CHMFL-VEGFR2-002 increased the animal survival compared with vehicle group.

3. Conclusions

Taken together, we discovered a novel highly selective inhibitor of VEGFR2 with good anti-angiogenic efficacy and safety, although its potency could be further improved. Unlike existing VEGFR2 inhibitors, CHMFL-VEGFR2-002 is a highly selective VEGFR2 inhibitor and has no activity against many other kinases, such as RET and c-KIT. CHMFL-VEGFR2-002 provides a potential antineoplastic drug candidate and a research tool for the study of anti-angiogenesis process.

4. Experimental

4.1. Synthetic route of compound CHMFL-VEGFR2-002

All solvents and reagents were used as obtained. ^1H NMR and ^{13}C NMR spectra were recorded with a Bruker 500 MHz NMR spectrometer (Karlsruhe, Germany) and referenced to deuterium dimethyl sulfoxide ($\text{DMSO-}d_6$). Chemical shifts are expressed in ppm. In the NMR tabulation, s indicates singlet; d, doublet; t, triplet; q, quartet; m, multiplet; and br, broad peak. LC/MS experiments were performed on an Agilent 6224 TOF (Santa Clara, CA, USA) using an ESI source coupled to an Agilent 1260 Infinity HPLC system operating in reverse mode with an Agilent Eclipse Plus C18 1.8 μm , 3.0 mm \times 50 mm column. Purification of the final compounds were performed with an Isco CombiFlash Rf⁺ system (Lincoln, NE, USA) (silica flash column 4 g) using a gradient of 0%–10% MeOH in DCM over 20 min at a flow rate of 18 mL/min. The purities of all final compounds were above 95%.

4.1.1. 6-Iodo-1H-indazol-3-amine (2)

Hydrazine (1.13 g, 35.3 mmol) was dissolved in butyl alcohol (80 mL) and treated with 2-fluoro-4-iodobenzonitrile (5.8 g,

23.5 mmol). The resulting solution was stirred at 115 $^{\circ}\text{C}$ for 5 h. Upon removal from heat, a white solid precipitated. This solid was collected by filtration and washed with isopropyl alcohol then diethyl ether and dried *in vacuo* at 50 $^{\circ}\text{C}$ to give the title compound as a white solid (4.5 g, 74%). ^1H NMR (500 MHz, $\text{DMSO-}d_6$) δ 11.45 (s, 1H), 7.62 (s, 1H), 7.50 (d, $J = 8.3$ Hz, 1H), 7.18 (d, $J = 8.3$ Hz, 1H), 5.43 (s, 2H); ^{13}C NMR (125 MHz, $\text{DMSO-}d_6$) δ 149.88, 143.08, 126.23, 122.71, 118.43, 113.80, 93.04; LC-MS (ESI, m/z) 259.97 [$\text{M} + \text{H}$]⁺.

4.1.2. 2-((3-Amino-1H-indazol-6-yl)thio)-N-methylbenzamide (3)

To a mixture of **2** (3.8 g, 14.6 mmol) and DMF (20 mL) were added methyl 3-mercaptopropionate (2.9 g, 1.75 mmol), Na_2CO_3 (3.1 g, 29.2 mmol), xantphos (0.23 g, 0.4 mmol) and $\text{Pd}_2(\text{dba})_3$ (1.4 g, 1.5 mmol). The reaction mixture was placed into an oil bath preheated to 80 $^{\circ}\text{C}$ and stirred at this temperature for 14 h under argon. Then the reaction mixture was cooled to room temperature before pouring into water (200 mL) a brown solid precipitates out. This solid was collected by filtration and washed with DCM and dried *in vacuo* at r.t. to give the title compound as a brown solid (3.1 g, 70%). ^1H NMR (500 MHz, $\text{DMSO-}d_6$) δ 11.49 (s, 1H), 8.35 (d, $J = 4.4$ Hz, 1H), 7.69 (t, $J = 7.5$ Hz, 1H), 7.45 (dd, $J = 7.5, 1.3$ Hz, 1H), 7.31–7.24 (m, 2H), 7.22 (dd, $J = 7.3, 6.6$ Hz, 1H), 6.94 (d, $J = 7.9$ Hz, 1H), 6.88 (dd, $J = 8.3, 1.1$ Hz, 1H), 5.43 (s, 2H), 2.77 (s, 3H); ^{13}C NMR (125 MHz, $\text{DMSO-}d_6$) δ 166.20, 160.65, 147.62, 140.13, 134.87, 129.78, 128.48, 127.63, 125.99, 123.99, 120.54, 119.78, 112.56, 111.92, 24.42. LC-MS (ESI, m/z) 299.10 [$\text{M} + \text{H}$]⁺.

4.1.3. 2-((3-Acetamido-1H-indazol-6-yl)thio)-N-methylbenzamide (CHMFL-VEGFR2-002)

To a solution of **3** (300 mg, 1 mmol) in DMF (5 mL) were added DIEPA (451.5 mg, 3.5 mmol). The mixture was stirred at 0 $^{\circ}\text{C}$ then acetyl chloride (235.5 mg, 3 mmol) was added. The resulting mixture was stirred at room temperature for 8 h. Then it was diluted with EtOAc (50 mL), washed with water (100 mL \times 3)

and brine (100 mL). The organic layers were dried over anhydrous sodium sulfate and concentrated. The residue was diluted with THF (10 mL) and 1,2-DAP (0.5 mL, 6 mmol). The reaction mixture was stirred at 60 °C for 4 h and then diluted with EtOAc (50 mL), washed with water (50 mL × 3) and brine (50 mL). The organic layers were dried over sodium sulfate, filtered, concentrated and purified by silica gel column chromatography (eluting with 0%–5% MeOH in DCM) to afford CHMFL-VEGFR2-002 (184 mg, 54%) as a white solid. ¹H NMR (500 MHz, DMSO-*d*₆) δ 12.71 (s, 1H), 10.42 (s, 1H), 8.37 (d, *J* = 4.5 Hz, 1H), 7.80 (d, *J* = 8.5 Hz, 1H), 7.54–7.39 (m, 2H), 7.36–7.22 (m, 2H), 7.00 (d, *J* = 8.0 Hz, 2H), 2.77 (d, *J* = 4.6 Hz, 3H), 2.10 (s, 3H); ¹³C NMR (125 MHz, DMSO-*d*₆) δ 168.85, 168.31, 141.90, 141.07, 137.28, 136.28, 132.77, 130.71, 130.27, 128.20, 126.48, 124.27, 124.11, 116.07, 114.80, 26.55, 23.33; LC–MS (ESI, *m/z*) 341.11 [M + H]⁺.

4.2. Expression and purification of human VEGFR-2-CD from SF9 cells

The catalytic domain (amino acids 786–1356) of human VEGFR-2 was PCR amplified from a cDNA library prepared from a mix of human cancer cell lines, and cloned into pFastBac HTA vector (Invitrogen, Carlsbad, CA, USA). The recombinant bacmid was transfected into SF9 by cellfectin (Invitrogen). The protein was expressed by infecting SF9 cells and protein purification was done following the previous protocol²⁷.

4.3. ADP-Glo biochemical assay

The ADP-Glo kinase assay (Promega, Madison, WI, USA) was used to screen for VEGFR2 inhibition of CHMFL-VEGFR2-002. The kinase reaction system contains 3 μL VEGFR 2 (40 ng/μL), 3 μL of serially diluted CHMFL-VEGFR2-002, 3 μL of substrate poly(4:1 Glu, Tyr) peptide (1.2 μg/μL) (Promega), and 3 μL of 200 μmol/L ATP (Promega). The reaction in each tube was started immediately by addition of ATP and maintained at 37 °C for 1 h. 12 μL of ADP-Glo reagent was then added to each well to stop the reaction and consume the remaining ATP in 40 min. Finally, 10 μL of the kinase assay reagent was added to the wells and incubated for 30 min to generate a luminescent signal. Luminescence signals were measured using an automated plate reader (Envision, PE, USA) and dose-response curves were fitted using Prism 5.0 (GraphPad Software Inc, San Diego, CA, USA).

4.4. Cell culture

The permanently transformed BaF3 cell line and MKN45 cell line were cultured in RPMI 1640 medium (Corning, Corning, NY, USA) containing 10% fetal calf serum (FBS) and supplemented with 2% L-glutamine 1% penicillin/streptomycin. The BaF3 cell line was incubated with 1 ng/mL IL-3, 10% fetal bovine serum (FBS) in RPMI 1640 medium (Corning) and supplemented with 2% L-glutamine 1% penicillin/streptomycin. Human Umbilical Vein Endothelial Cell (HUVEC) cell lines were purchased from the American Type Culture Collection (Rockefeller, Maryland, MD, USA) and cultured in vascular cell basal medium containing endothelial cell growth kit-VEGF, 10% FBS, 2% L-glutamine, and 1% penicillin/streptomycin. All cell lines were maintained in medium at 37 °C and 5% CO₂.

4.5. BaF3 isogenic cell line generation

MSCV-based retroviral expression vectors and transgenic BaF3 cell lines were constructed as previously described.²⁸

4.6. Anti-proliferation assay

The cells were grown in 96-well plates (1800 cells/well) and various concentrations of compounds were added. Cell proliferation was measured after 72 h of treatment with the compound. CCK8 assay was performed according to the manufacturer's instructions and measured in a microplate reader (Bio-Rad, Hercules, CA, USA). Data were normalized to control (DMSO) and GI₅₀ values were calculated using Prism 5.0 (GraphPad Software Inc).

4.7. Antibodies and immunoblotting

The following antibodies were purchased from Cell Signaling Technology (Danvers, MA, USA): VEGFR2 antibody (#9698), phospho-VEGFR2 (Tyr951) antibody (#4991), phospho-VEGFR2 (Tyr996) antibody (#2474), phospho-VEGFR2 (Tyr1059) antibody (#3817), phospho-VEGFR2 (Tyr1175) antibody (#3770), PDGFRA antibody (#3174), phospho-PDGFR (Tyr754) antibody (#2992), PDGFRB antibody (#4564), phospho-PDGFRB (Tyr857) antibody (#3170). All the antibodies were used at a dilution of 1:1000 in immunoblotting.

4.8. The Cellular Thermal Shift Assay (CETSA)

Cells were pre-treated with the compound of indicated concentrations for 1 h. Cells were collected and transferred to PCR tubes for incubation at different temperatures for 3 min. Samples were then treated with three freeze/thaw cycles in liquid nitrogen. Insoluble proteins were separated by centrifugation, and the soluble proteins were analyzed using Western blotting.

4.9. Molecular modeling

All calculations were performed using the Schrödinger Suite (LLC, New York, NY, USA). The VEGFR2 complex (PDB ID: 4AG8) was used for docking studies. The crystal structure was prepared using the Protein Preparation Wizard. The ligand structures were built in Maestro and prepared for docking using LigPrep (LigPrep 3.4, Schrödinger) and further docked into the receptor by the IFD protocol (Induced Fit Docking protocol, Schrödinger).

4.10. Tube formation assay

To investigate the effect of CHMFL-VEGFR2-002 on HUVEC tube formation, Matrigel (BD Biosciences, Lake Franklin, NJ, USA) was placed in pre-chilled 96-well plates (70 μL/well) and polymerized at 37 °C for 30 min. HUVEC cells suspended in complete medium was seeded on Matrigel at a density of 8 × 10³ cells/well with vehicle or CHMFL-VEGFR2-002. After 24 h of incubation, the tubular structure was observed under an optical microscope. Finally, network formation was quantified by the total length (pixels) of the branches using ImageJ image analysis software (<http://rsbweb.nih.gov/ij/>).

4.11. Wound healing assay

Monolayer HUVEC cells were seeded into 24-well plates and then injured with a yellow pipette tip. The cells were washed with PBS (pH 7.4). A new complete medium containing DMSO or different concentrations of CHMFL-VEGFR2-002 was added to the scratched monolayer. The plates were incubated for 24 h as above. Images were taken with an OLYMPUS digital camera (Tokyo, Japan) and analyzed by ImageJ (Bethesda, USA).

4.12. Transwell invasion assay

A transwell plate filter was coated with 40 μ L Matrigel (BD Biosciences) for 4 h at 37 °C. After Matrigel polymerization, 100 μ L of complete medium was filled in the bottom chamber, and 100 μ L of free FBS medium and 5×10^4 HUVEC were added to the top chamber. The top chamber contained DMSO or various concentrations of CHMFL-VEGFR2-002. After 24 h, the migrated cells were fixed with methanol and the non-migrating cells were scraped off with cotton. The migrated cells were then stained with 0.05% crystal violet and photographed under a light microscope.

4.13. Pharmacokinetics study

This study protocol was approved by the Hefei Institutes of Physical Science Ethics Committee (Hefei, China). The male Sprague–Dawley rats (200 g) were provided by Laboratory Animal Center of Anhui Medical University (Hefei, China). Pharmacokinetics study were performed as previously described²⁹.

4.14. Acute toxicity study

Study was performed in five-week-old ICR female mice purchased from Nanjing Biomedical Research Institute, Nanjing University (Nanjing, China), and was approved by the Hefei Institutes of Physical Science Ethics Committee, Chinese Academy of Sciences (Hefei, China). Animals were acclimatized to the facilities for three day and then fasted for 12 h with free access to water before experiment. 12 mice were randomly and equally divided into six groups for one compound's acute toxicity study with oral administration at doses of 0, 125, 250, 500, 1000 and 2000 mg/kg. The animals were observed for 7 days and their weights were recorded every day.

4.15. Drug studies in zebrafish

Transgenic zebrafish embryos were grown according to protocols in a standard environment³⁰. Zebrafish embryos are produced by natural pair mating (3–12 months old) and cultured in embryo water at 28.5 °C. Zebrafish embryos were collected and distributed into 12-well microplates with 15 fish in each well. Zebrafish embryos were incubated with CHMFL-VEGFR2-002, sunitinib or DMSO. Embryos treated in each well were then incubated at 28 °C for 72 h according to the assay. Embryos receiving DMSO (0.1%) served as a vehicle control, equivalent to no treatment. Imaging was performed using ImageXpress Micro (Molecular Device, San Jose, CA, USA).

4.16. Mice models

All animal experiments were performed in five-week-old female mice purchased from Nanjing Biomedical Research Institute,

Nanjing University (Nanjing, China), and all *in vivo* studies were approved by the Hefei Institutes of Physical Science Ethics Committee, Chinese Academy of Sciences (Hefei, China). 1×10^6 MKN45 cells in PBS were prepared and intraperitoneally inoculated into nude mice. Oral administration was started daily after inoculation. To assess the anti-tumor activity of CHMFL-VEGFR2-002, mice were sacrificed on day 17 and autopsied. The number of tumors in the mesentery was counted.

In the survival study, 1×10^5 B16-F10 cells were prepared and intraperitoneally inoculated into C57 mice. Oral administration was started daily after inoculation. The date of death was recorded and analyzed by Prism 5.0 (GraphPad Software Inc.).

Acknowledgments

This work was supported by the National Natural Science Foundation of China (Grant Nos. 81773777, 81673469, 81603123, 81803366), the China Postdoctoral Science Foundation (Grant Nos. 2018T110634, 2018M630720), the Anhui Province Postdoctoral Science Foundation (Grant No. 2018B279), the CASH-IPS Director's Fund (Grant No. BJPY2019A03) and the Key Program of 13th five-year plan, CASHIPS (Grant No. KP-2017-26).

Author contributions

Qingsong Liu, Jing Liu, Guangchen Hong and Zongru Jiang designed experiments; Zongru Jiang, Li Wang, Xuesong Liu, Cheng Chen, Aoli Wang, Beilei Wang, Chen Hu and Wenliang Wang carried out experiments; Zongru Jiang, Beilei Wang, Wenliang Wang, Chen Hu, Kailin Yu, Ziping Qi, Qingwang Liu and Aoli Wang analyzed experimental results; Qingsong Liu, Jing Liu and Wenchao Wang wrote the manuscript.

Conflicts of interest

The authors have no conflicts of interest to declare.

Appendix A. Supporting information

Supporting data to this article can be found online at <https://doi.org/10.1016/j.apsb.2019.10.004>.

References

1. Carmeliet P, Jain RK. Angiogenesis in cancer and other diseases. *Nature* 2000;**407**:249–57.
2. Gotink KJ, Verheul HMW. Anti-angiogenic tyrosine kinase inhibitors: what is their mechanism of action?. *Angiogenesis* 2010;**13**:1–14.
3. Benjamin LE, Bergers G. Tumorigenesis and the angiogenic switch. *Nat Rev Cancer* 2003;**3**:401–10.
4. Kerbel RS. Tumor angiogenesis: past, present and the near future. *Carcinogenesis* 2000;**21**:505–15.
5. Kerbel R, Folkman J. Clinical translation of angiogenesis inhibitors. *Nat Rev Cancer* 2002;**2**:727–39.
6. Carmeliet P. VEGF as a key mediator of angiogenesis in cancer. *Oncology* 2005;**69**:4–10.
7. Hicklin DJ, Ellis LM. Role of the vascular endothelial growth factor pathway in tumor growth and angiogenesis. *J Clin Oncol* 2005;**23**:1011–27.

8. Orock ZK, Makarem JA, Shamseddine AI. Vascular endothelial growth factor family of ligands and receptors: review. *Blood Cell Mol Dis* 2007;**38**:258–68.
9. Ferrara N, Hillan KJ, Gerber HP, Novotny W. Discovery and development of bevacizumab, an anti-VEGF antibody for treating cancer. *Nat Rev Drug Discov* 2004;**3**:391–400.
10. Olsson AK, Dimberg A, Kreuger J, Claesson-Welsh L. VEGF receptor signaling—in control of vascular function. *Nat Rev Mol Cell Biol* 2006;**7**:359–71.
11. Yu Y, Cai W, Pei C, Shao Y. Rhamnazin, a novel inhibitor of VEGFR2 signaling with potent antiangiogenic activity and antitumor efficacy. *Biochem Biophys Res Commun* 2015;**458**:913–9.
12. Fontanella C, Ongaro E, Bolzonello S, Guardascione M, Fasola G, Aprile G. Clinical advances in the development of novel VEGFR2 inhibitors. *Ann Transl Med* 2014;**2**:123.
13. di Marco V, de Vita F, Koskinas J, Semela D, Toniutto P, Verslype C. Sorafenib: from literature to clinical practice. *Ann Oncol* 2013;**24**:ii30–7.
14. Geng R, Li J. Apatinib for the treatment of gastric cancer. *Expert Opin Pharmacother* 2015;**16**:117–22.
15. Obi S, Sato T, Sato S, Kanda M, Tokudome Y, Kojima Y, et al. The efficacy and safety of lenvatinib for advanced hepatocellular carcinoma in a real-world setting. *Hepatol Int* 2019;**13**:199–204.
16. Molina AM, Hutson TE, Nosov D, Tomczak P, Lipatov O, Sternberg CN, et al. Efficacy of tivozanib treatment after sorafenib in patients with advanced renal cell carcinoma: crossover of a phase 3 study. *Eur J Cancer* 2018;**94**:87–94.
17. Soria JC, DeBraud F, Bahleda R, Adamo B, Andre F, Dientsmann R, et al. Phase IIIa study evaluating the safety, efficacy, pharmacokinetics, and pharmacodynamics of lucitanib in advanced solid tumors. *Ann Oncol* 2014;**25**:2244–51.
18. Wang F, Molina J, Satele D, Yin J, Lim VS, Adjei AA. A phase I study of the vascular endothelial growth factor inhibitor vatalanib in combination with pemetrexed disodium in patients with advanced solid tumors. *Invest New Drugs* 2019;**37**:658–65.
19. Wolter P, Dumez H, Schöffski P. Sunitinib and hypothyroidism. *N Engl J Med* 2007;**356**:1580–1.
20. Fife DJ, Wu JJ, Behnam SE, Linden KG. Sunitinib-induced hand-foot syndrome: a new, distinct form. *Clin Exp Dermatol* 2009;**35**:200–1.
21. Desai J, Yassa L, Marqusee E, George S, Frates MC, Chen MH, et al. Hypothyroidism after sunitinib treatment for patients with gastrointestinal stromal tumors. *Ann Intern Med* 2006;**145**:660–4.
22. Rini BI, Tamaskar I, Shaheen P, Salas R, Garcia J, Wood L, et al. Hypothyroidism in patients with metastatic renal cell carcinoma treated with sunitinib. *J Natl Cancer Inst* 2007;**99**:81–3.
23. Rogiers A, Wolter P, Op de Beeck K, Thijs M, Decallonne B, Schöffski P. Shrinkage of thyroid volume in sunitinib-treated patients with renal-cell carcinoma: a potential marker of irreversible thyroid dysfunction?. *Thyroid* 2010;**20**:317–22.
24. McTigue M, Murray BW, Chen JH, Deng Y, Solowiej J, Kania RS, et al. Molecular conformations, interactions, and properties associated with drug efficiency and clinical performance among VEGFR TK inhibitors. *Proc Natl Acad Sci U S A* 2012;**109**:18281–9.
25. Lu J, Zhang K, Nam S, Anderson RA, Jove R, Wen W. Novel angiogenesis inhibitory activity in cinnamon extract blocks VEGFR2 kinase and downstream signaling. *Carcinogenesis* 2010;**31**:481–8.
26. Nakagawa T, Tohyama O, Yamaguchi A, Matsushima T, Takahashi K, Funasaka S, et al. E7050: a dual c-Met and VEGFR-2 tyrosine kinase inhibitor promotes tumor regression and prolongs survival in mice xenograft models. *Cancer Sci* 2010;**101**:210–5.
27. Kumar R, Crouthamel MC, Rominger DH, Gontarek RR, Tummino PJ, Levin RA, et al. Myelosuppression and kinase selectivity of multikinase angiogenesis inhibitors. *Br J Cancer* 2009;**101**:1717–23.
28. Wang A, Wu H, Chen C, Hu C, Qi Z, Wang W, et al. Dual inhibition of AKT/FLT3-ITD by A674563 overcomes FLT3 ligand-induced drug resistance in FLT3-ITD positive AML. *Oncotarget* 2016;**7**:29131–42.
29. Wu Y, Wang B, Wang J, Wang J, Qi S, Zou F, Qi Z, et al. Discovery of 2-(4-chloro-3-(trifluoromethyl)phenyl)-N-(4-((6,7-dimethoxyquinolin-4-yl)oxy)phenyl)acetamide (CHMFL-KIT-64) as a novel orally available potent inhibitor against broad-spectrum mutants of c-KIT kinase for gastrointestinal stromal tumors. *J Med Chem* 2019;**62**:6083–101.
30. Kimmel CB, Ballard WW, Kimmel SR, Ullmann B, Schilling TF. Stages of embryonic development of the zebrafish. *Dev Dyn* 1995;**203**:253–310.